ELSEVIER

Contents lists available at ScienceDirect

Nuclear Inst. and Methods in Physics Research, B

journal homepage: www.elsevier.com/locate/nimb





Multiply-charged argon ion irradiation of microfabricated niobium wires

Bernardo Langa Jr. ^a, Ivan Lainez ^a, Margaret Marte ^a, Patrick Johnson ^a, Neil Mehta ^b, Dhruva Kulkarni ^b, Mohan Ghimire ^a, Dale Hensley ^c, Bernadeta Srijanto ^c, Chad Sosolik ^a, Kasra Sardashti ^{a,d,*}

- ^a Department of Physics & Astronomy, Clemson University, Clemson, SC, United States
- ^b NERSC, Lawrence Berkeley National Laboratory, Berkeley, CA, United States
- ^c Center for Nanophase Materials, Oak Ridge National Laboratory, Oak Ridge, TN, United States
- d Department of Physics, University of Maryland, College Park, MD, United States

ARTICLE INFO

Keywords: Superconductivity Micro-devices Multiply-charged ions Irradiation

ABSTRACT

While rare on Earth, multiply-charged ions (MCIs) are abundant species in outer space. For spacecraft outside the Earth's atmosphere, MCIs are some of the main contributors to the failure of electronic devices. While the detrimental effects of MCIs on space electronics have been known for quite some time, the underlying physics of their interactions, which are tied to the coupling of both electronic and lattice degrees of freedom, are complex and remain relatively unexplored. The impacts of MCIs on superconducting electronics used for detection and communication in outer space are particularly unknown. Here, we aim to shed light on such interactions by examining the effect of low- to medium-dose Ar⁸⁺ irradiation on the physical characteristics (e.g., surface topography, electrical transport) of microfabricated niobium (Nb) wires.

1. Introduction

Multiply-charged ions (MCIs) are a unique form of matter defined as ionized atoms that are missing two or more electrons, which means they possess partially, or even completely, unscreened nuclei and intense electric fields associated with their charge [1,2]. Such ions are extremely rare on Earth, but they are plentiful in space beyond Earth's magnetosphere, primarily found as charged components of the solar wind [3–5]. There is a direct coupling of the magnetosphere to the solar wind through fluctuations in the wind's speed and density, which allows the position of the sphere's protective boundary or magnetopause to shift dramatically. Therefore, it is not uncommon for shifts in the magnetopause by up to several Earth radii exposes man-made objects such as geosynchronous satellites directly to the solar wind and, hence, to MCIs.

The Advanced Composition Explorer (ACE) system's Solar Wind Ion Composition Spectrometer (SWICS) measurements have shown that the heavy components of the solar wind are elements such as Si, O, and Fe in highly charged ionic states [6]. The potential energies of such ions, which correspond to the sum of the ionization energies of the element up to its charge state, range from 1.369 keV for Si⁴⁺ to 1.166 keV for O⁷⁺ and 0.549 keV for Fe⁸⁺. It should be noted that MCI components of the solar wind constitute no more than 1 % of the total constituents [7].

However, if one considers that these ions have kinetic energies that fall in the range of 5 keV to 185 keV, it is clear that the combined damage that each component (kinetic plus potential) can inflict on exposed parts in the space environment is severe. Additionally, the deexcitation processes that are initiated when a multicharged ion contacts a surface include neutralizing not only electrons but also secondary X-ray emissions from the ions [8,9].

Superconducting electronics, particularly superconducting detectors, are often considered the best candidates for the detection of radiation in the form of particles and electromagnetic waves over a broad energy range, with high energy and time resolution [10,11]. As quantum sensors, a superconducting detector should discriminate single events within the period of arrival and collision with the surface. Superconducting single-particle detectors (SSPDs) with nano-striplines are particularly useful for charged particle detection studies in outer space thanks to their very fast response time and high detection resolution [10,12,13]. SSPDs can, in principle, also be used for high-fidelity detection of MCIs. However, the impact of MCI radiation on superconducting materials and devices is not known. Detailed investigations of the SSPDs in terrestrial beamlines is essential in shedding light on the underlying mechanisms of MCI-superconductor interactions.

Here, we present the first study of the impact MCI irradiation has on

^{*} Corresponding author at: Department of Physics, University of Maryland, College Park, MD 20740, United States. E-mail address: ksardash@umd.edu (K. Sardashti).

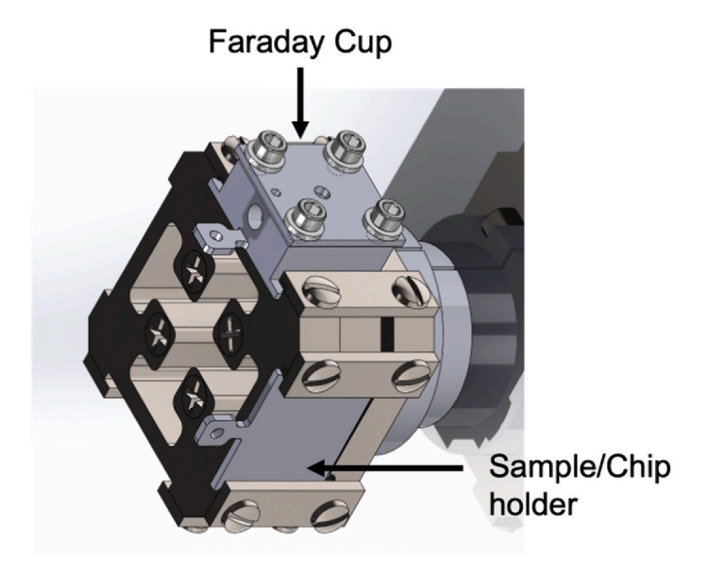


Fig. 1. Figure of the 4-sample holder and Faraday cup.

the physical characteristics of superconducting micro-devices. We utilized ${\rm Ar}^{8+}$ as our model ion with acceleration energies of 36 keV and fluences as high as 3.66 x 10^{15} cm $^{-2}$. Niobium microwires are used as common superconducting devices that can be readily integrated into future MCI detectors. Using atomic force microscopy and cryogenic transport measurements, we monitor the impact of low to medium ${\rm Ar}^{8+}$ on Nb microwires' surface topology and electrical properties. Sputtering effects are calculated from a change in the resistance of the films before and after irradiation and agree well with simulated results from the Stopping and Range of Ions in Matter (SRIM) software. These results may be used to guide future experiment design.

2. Experimental details

The superconducting microwires were fabricated from 200 nm thick Nb films deposited via DC sputtering at 3 mTorr of Ar carrier gas. The Nb film was deposited on a 4-in semi-insulating Si(001) wafer that underwent RCA clean (developed by the Radio Corporation of America) and oxide etch (using buffer oxide etchant solution). The Nb/Si wafer was then patterned into an array of microwires using electron beam lithography (JEOL 8100 FS E-Beam). Each cell of the array consisted of patterns for four microwires of 90 μ m, 60 μ m, 30 μ m, and 10 μ m in width.

The microwires were then realized through reactive ion etching using an SF_6/Ar etching, followed by resist removal. The Si wafer was then diced into $1 \times 1 \text{ cm}^2$ chips that included single cells with four microwires each.

The MCI irradiation experiments on the Nb microwire chips were carried out at the Clemson University Electron Beam Ion Trap (CU-EBIT) beamline. The irradiation station consists of a rotatable 4-sample holder (Fig. 1). One face has a Faraday cup (FC3) mounted in an equivalent position to the sample. The Nb microwire chip was mounted on one of the other three positions of the holder. The Ar⁸⁺ beam was tuned into the FC3, and a HeNe laser was used to confirm the ion beam alignment by directing the laser into the aperture for the FC3. The kinetic energy of the beam was set to 4.5 keV/Q (equal to 36 keV for Ar⁸⁺ ions). The irradiation procedure consisted of first tuning the ion beam into the FC3 and monitoring the beam for stability. Upstream of FC3 is another Faraday cup (FC2), which can be lowered to block the beam, as well as to measure the beam current intermittently throughout the sample exposure process. Once the beam is considered stable, the sample holder is rotated such that the laser is incident on the appropriate section of the sample.

We evaluated the nanoscale surface topography of the Nb films and microwires before and after each exposure step using atomic force microscopy (AFM Workshop HR-2D). The AFM uses a silicon tip in vibrational mode to scan across the sample surface in areas as large as $50 \times 50 \ \mu m^2$. Furthermore, we monitored the electrical properties of the microwires by measuring the differential resistance (dV/dI) vs. temperature, magnetic field (applied perpendicular to the chips), and DC bias current. The dV/dI signals were acquired in 4-point geometry via lock-in amplifiers with an AC excitation current of $100 \ \mu A$. All electrical transport measurements were performed in a cryogen-free refrigerator (Oxford Instruments Teslatron PT) with a base temperature of $1.5 \ K$ and a maximum single-axis magnetic field of $12 \ T$.

3. Results & discussion

The Nb microwires were exposed to the ${\rm Ar}^{8+}$ beam in 3 steps. The cumulative ion doses after steps 1 to 3 of the exposure were 5.39×10^{13} cm $^{-2}$, 6.78×10^{14} cm $^{-2}$, and 3.66×10^{15} cm $^{-2}$, respectively. Fig. 2 displays $2.5 \,\mu m \times 2.5 \,\mu m$ nanoscale topographical maps for $10 \,\mu m$ wide Nb microwires as-deposited and after each of the 3 exposure steps. The as-deposited devices showed a fine-grained structure consistent with previous studies on sputtered Nb thin films [14,15]. Several pinholes (seen as black dots in the maps) emerged after the first step of the irradiation and persisted throughout the following steps, while the Nb grain structure was preserved in the matrix. The ${\rm Ar}^{8+}$ irradiation also

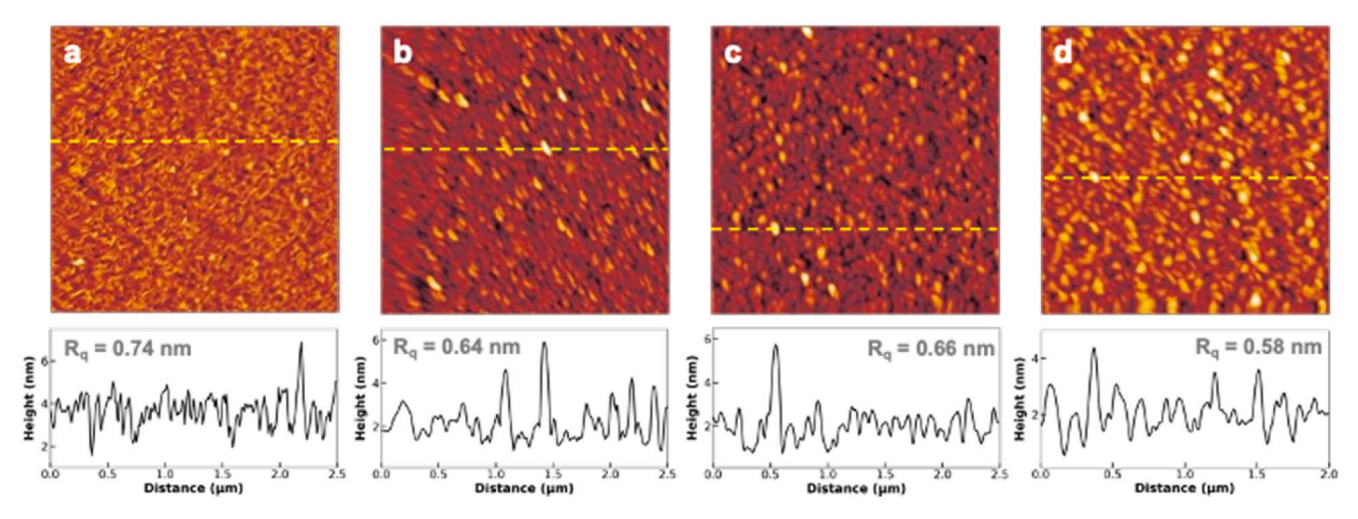


Fig. 2. Surface topography of the Nb microwires as a function of Ar^{8+} exposure dose: (a) As-fabricated with no exposure; (b) 5.39 x 10^{13} cm⁻²; (c) 6.78 x 10^{14} cm⁻²; (d) 3.66 x 10^{15} cm⁻².

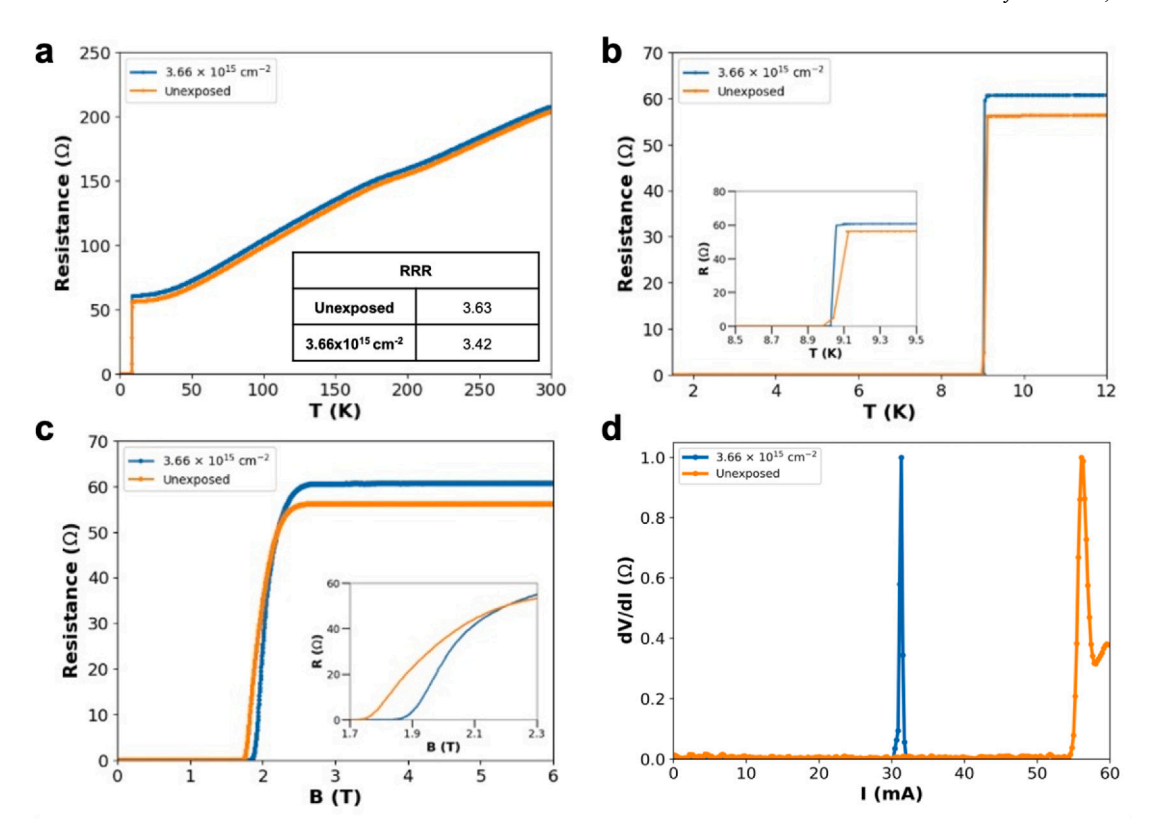


Fig. 3. The electrical characteristics of a 10 μ m wide Nb microwire as-fabricated (orange) and after Ar⁸⁺ exposure dose of 3.66 x 10¹⁵ cm⁻²: (a) resistance vs. temperature from room temperature down to 1.5 K; (b) resistance vs. temperature near the superconducting transition region; (c) resistance vs. magnetic field applied perpendicular to the chip's surface; (d) differential resistance vs. DC bias current to determine the critical current (I_c).

reduced the root-mean-square roughness (R_q) of the samples by 0.1 nm after the first exposure, followed by another 0.06 nm reduction after the last step. This is consistent with the gradual sputtering of Nb atoms from the microwires' top surface leading to a smoother structure.

The changes in the surface topography can lead to detectable shifts in the transport properties of the Nb microwires. Fig. 3 shows the superconducting transport characteristics of a 10 µm wide Nb wire in an asdeposited state and after all 3 steps of Ar⁸⁺ exposure (dose of 3.66 x 10^{15} cm $^{-2}$). Fig. 3a shows the resistance vs. temperature for the Nb microwire from 300 K to 1.5 K before and after 3 steps of exposure. The residual resistance ratio (RRR= $R_{300\mbox{\scriptsize K}}/R_{10\mbox{\scriptsize K}}$) for each condition is provided in the inset table. The Ar⁸⁺ exposure resulted in a slight decrease in the RRR, which could be attributed to a more disordered film structure due to sputtering. The superconducting transition for the Nb microwire occurs at around 9 K, with the Ar⁸⁺ exposure only reducing the onset of the transition by 0.1 K (Fig. 3b), which is within the margins of error for such measurements. Fig. 3c shows the superconductornormal (S-N) transition in the 10-µm Nb microwire as a function of the out-of-plane magnetic field. Ar⁸⁺ radiation has a small effect on the critical magnetic field (B_c) as it shifts the onset of S-N transition to higher fields by 0.15 T. This is consistent with thinning the Nb microwires. The effect of radiation, however, is most significant on the critical current of the microwires, as shown in Fig. 3d, where the microwire's differential resistance (dV/dI) is plotted as a function of DC current bias. The 3-step exposure reduced the critical current (I_c) from 54.78 mA to 30.43 mA, a significant shift that could not be accounted for solely by the thinning of the channel through sputtering.

It is necessary to investigate sputtering effects to constrain irradiation parameters in future measurements. The enhanced sputtering effects of MCIs on bulk insulators and semiconductor substrates are well known, [16] but are not observed in bulk metallic samples due to the abundance of free electrons available to shield any electron–phonon coupling effects. However, in the nanometer regime, enhanced

sputtering due to charge state effects has been observed [17,18].

We have carried out pre- and post-irradiation four-point probe measurements on our samples to estimate the sputter yield for multiply-charged ion irradiation. The resistance R of a microwire depends on the sputtering yield s according to:

$$R = \frac{\rho l}{w(t_0 - \frac{s dv}{wl})} \tag{1}$$

where ρ is the resistivity, l is the length in the direction of the current of the four-point probe, t_0 is the initial thickness in the direction along the ion beam irradiation, w is the dimension orthogonal to length and thickness, d denotes the fluence of the ion beam (or dose), and v is the atomic volume of each target atom (i.e., Nb). For approximate calculations, we have assumed that the sputtering effect is uniform across the film and neglected the effect of implanted ions on the resistivity and the atomic volume. A plot of 1/R vs. the fluence d is expected to be linear for doses that have not yet resulted in complete removal of the thin film [19], with a slope m that can be used to calculate the sputter yield according to:

$$s = \frac{\rho l^2 |m|}{\nu} \tag{2}$$

The four-point measurements were conducted before and after the multiple dosing steps for a cumulative fluence of 3.66 x 10^{15} per cm² and resulted in an increase in measured resistance from 203.8 Ω to 207.53 Ω (resulting in a slope $|\textbf{\textit{m}}|$ of 1.20 x 10^{-16}). Using 1.5 x 10^{-5} Ω .cm for ρ , 0.2 nm as the atomic radius (to calculate the atomic volume), and 2 mm and 10 μ m for $\textbf{\textit{l}}$ and $\textbf{\textit{w}}$, respectively, we obtain an estimated sputtering yield of 2.16 atoms/ion.

To model our experimental results, we have used the well-known Monte Carlo simulation package SRIM [20]. Sputtering yield for a target consisting of a 200 nm Nb thin film grown on bulk Si (simulated as

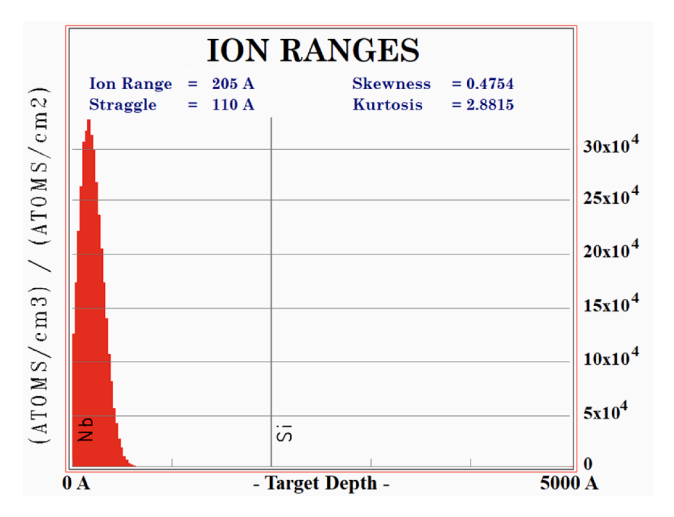


Fig. 4. The implantation depth of Ar^+ ions at 36 keV in a simulated 200 nm Nb film grown on a Si substrate as obtained from the SRIM package.

1000 nm Si layer) irradiated with singly charged Ar⁺ in the "monolayer collisions steps" calculation mode was employed for ion kinetic energies of 10 keV, 36 keV, and 50 keV. Ions penetrate to the first 20 nm of the Nb film, as shown in Fig. 4. We expect the implantation range for the multiply charged argon ions to be lower than (or equal to) that of the singly charged ions due to possible enhanced stopping effects.

Surface binding energies estimated from the sublimation energy at room temperature were used by default, and the resultant sputter yield was approximately 2.5 atoms/ion for the kinetic energies considered, which compares well with our experimental number (2.16) above.

The effects of the charge state of MCIs on the stopping power and, consequently, the sputtering cross-sections are not yet included in popular Monte-Carlo Binary Collision Approximation (BCA) packages. We note that even while considering only singly charged ions, various binary collision approximation codes (SRIM, TRIDYN, SDTrimSP) are at odds with each other when estimating sputtering data, as reported here [21,22]. Additionally, at lower kinetic energies, which may be necessary to separate potential energy effects from kinetic energy effects in future experiments, collective surface effects are more prominent, and tools like molecular dynamics (MD) may be used to capture these effects with greater accuracy. We plan to run in-silico sputtering experiments using MD to measure yields and compare them to existing data.

4. Conclusions

We presented the first study examining the impact of MCI irradiation on the physical properties of superconducting micro-devices. We employed Nb microwires as our model system and $\mathrm{Ar^{8^+}}$ at 36 keV as our model MCI for the irradiation studies. We found that a moderate dose of $\mathrm{Ar^{8^+}}$ (3.66 x 10^{15} cm $^{-2}$) leads to decreased RMS roughness in the microwires, achieved through sputtering. The changes in the transport characteristics of the Nb microwires supported this observation: a slight increase in the critical magnetic field and a notable decrease in the critical current. SRIM modeling confirmed that our experimental doses could produce the sputtering yields necessary to create such detectable changes in superconducting transport properties.

Declaration of competing interest

The authors declare that they have no known competing financial interests or personal relationships that could have appeared to influence the work reported in this paper.

Acknowledgments

The Clemson team is supported by AFOSR grant no. FA9550-23-1-0419 and DOE grant no. DE-SC0023595. Fabrication of Nb bars was conducted as part of a user project at the Center for Nanophase Materials Sciences (CNMS), which is a US Department of Energy, Office of Science User Facility at Oak Ridge National Laboratory.

References

- [1] J.D. Gillaspy, Highly charged ions, J. Phys. B at. Mol. Opt. Phys. 34 (19) (Sep. 2001) R93–R130, https://doi.org/10.1088/0953-4075/34/19/201.
- [2] M. G. Kozlov, M. S. Safronova, J. R. Crespo López-Urrutia, and P. O. Schmidt, "Highly charged ions: Optical clocks and applications in fundamental physics," *Rev. Mod. Phys.*, vol. 90, no. 4, p. 045005, Dec. 2018, doi: 10.1103/ RevModPhys.90.045005.
- [3] T.E. Cravens, X-ray Emission from Comets, Science 296 (5570) (May 2002) 1042–1045, https://doi.org/10.1126/science.1070001.
- [4] M. Neugebauer, et al., The relation of temporal variations of soft X-ray emission from comet Hyakutake to variations of ion fluxes in the solar wind, J. Geophys. Res. Space Phys. 105 (A9) (2000) 20949–20955, https://doi.org/10.1029/ 1999 14000299
- [5] S. Otranto, R.E. Olson, P. Beiersdorfer, X-ray emission cross sections following charge exchange by multiply charged ions of astrophysical interest, Phys. Rev. A 73 (2) (Feb. 2006) 022723, https://doi.org/10.1103/PhysRevA.73.022723.
- [6] G. Gloeckler et al., "The Solar Wind Ion Composition Spectrometer," Astron. Astrophys. Suppl. Ser., vol. 92, no. 2, pp. 267–289, Jan. 1992, Accessed: Jan. 06, 2022. [Online]. Available: https://ui.adsabs.harvard.edu/abs/1992A&AS...92..267G/abstract.
- [7] G. Gloeckler et al., "Investigation of the Composition of Solar and Interstellar Matter Using Solar Wind and Pickup Ion Measurements with SWICS and SWIMS on the Ace Spacecraft," in *The Advanced Composition Explorer Mission*, C. T. Russell, R. A. Mewaldt, and T. T. Von Rosenvinge, Eds., Dordrecht: Springer Netherlands, 1998, pp. 497–539. doi: 10.1007/978-94-011-4762-0_18.
- [8] H. Kurz, K. Töglhofer, H.P. Winter, F. Aumayr, R. Mann, Electron emission from slow hollow atoms at a clean metal surface, Phys. Rev. Lett. 69 (7) (Aug. 1992) 1140–1143, https://doi.org/10.1103/PhysRevLett.69.1140.
- [9] H. Winter, F. Aumayr, Hollow atoms, J. Phys. B at. Mol. Opt. Phys. 32 (7) (Jan. 1999) R39–R65, https://doi.org/10.1088/0953-4075/32/7/005.
- [10] R. Cristiano, M. Ejrnaes, A. Casaburi, N. Zen, M. Ohkubo, Superconducting nanostrip particle detectors, Supercond. Sci. Technol. 28 (12) (Dec. 2015) 124004, https://doi.org/10.1088/0953-2048/28/12/124004.
- [11] S. Miki, M. Takeda, M. Fujiwara, M. Sasaki, A. Otomo, Z. Wang, Superconducting NbTiN nanowire single photon detectors with low kinetic inductance, Appl. Phys. Express 2 (7) (Jun. 2009) 075002, https://doi.org/10.1143/APEX.2.075002.
- [12] A. Casaburi, et al., A 2 × 2 mm ² superconducting strip-line detector for high-performance time-of-flight mass spectrometry, Supercond. Sci. Technol. 25 (11) (Nov. 2012) 115004, https://doi.org/10.1088/0953-2048/25/11/115004.
- [13] A. Casaburi, M. Ejrnaes, R. Cristiano, 1 mm ultrafast superconducting stripline molecule detector, Appl. Phys. Lett. 95 (17) (Oct. 2009) 172508, https://doi.org/ 10.1063/1.3256220.
- [14] T. Tachiki, K. Horiguchi, T. Uchida, Fabrication of Niobium Nanobridge Josephson Junctions, J. Phys. Conf. Ser. 507 (4) (May 2014) 042041, https://doi.org/ 10.1088/1742-6596/507/4/042041.
- [15] D. Bromley et al., "Electron beam evaporation of superconductor-ferromagnet heterostructures," Sci. Rep., vol. 12, no. 1, Art. no. 1, May 2022, doi: 10.1038/ s41598-022-11828-v.
- [16] T. Schenkel, et al., Charge state dependent energy loss of slow heavy ions in solids, Phys. Rev. Lett. 79 (11) (Sep. 1997) 2030–2033, https://doi.org/10.1103/ PhysRevLett.79.2030.
- [17] J.M. Pomeroy, A.C. Perrella, H. Grube, J.D. Gillaspy, Gold nanostructures created by highly charged ions, Phys. Rev. B 75 (24) (Jun. 2007) 241409, https://doi.org/ 10.1103/PhysRevB.75.241409.
- [18] G.L. Szabo, et al., Charge-state-enhanced ion sputtering of metallic gold nanoislands, Small 19 (26) (2023) 2207263, https://doi.org/10.1002/ smll.202207263.
- [19] J.K. Steele, C.H. Koch, D.I. Potter, Self-ion sputtering yield determinations of (100) nickel thin films, Surf. Coat. Technol. 51 (1) (Apr. 1992) 399–404, https://doi.org/10.1016/0257-8972(92)90271-B.
- [20] J.P. Biersack, L.G. Haggmark, A Monte Carlo computer program for the transport of energetic ions in amorphous targets, Nucl. Instrum. Methods 174 (1) (Aug. 1980) 257–269, https://doi.org/10.1016/0029-554X(80)90440-1.
- [21] Q. Nénon, A. R. Poppe, A. Rahmati, and J. P. McFadden, "Implantation of Martian atmospheric ions within the regolith of Phobos," *Nat. Geosci.*, vol. 14, no. 2, Art. no. 2, Feb. 2021, doi: 10.1038/s41561-020-00682-0.
- [22] H. Hofsäss, K. Zhang, A. Mutzke, Simulation of ion beam sputtering with SDTrimSP, TRIDYN and SRIM, Appl. Surf. Sci. 310 (Aug. 2014) 134–141, https://doi.org/10.1016/j.apsusc.2014.03.152.